



Stabilization of Tryptophan Hydroxylase 2 by L-Phenylalanine Induced Dimerization

Tidemand, Kasper Damgaard; Christensen, Hans Erik Mølager; Hoeck, Niclas; Harris, Pernille; Boesen, Jane; Peters, Günther H.J.

Published in:
F E B S Open Bio

Link to article, DOI:
[10.1002/2211-5463.12100](https://doi.org/10.1002/2211-5463.12100)

Publication date:
2016

Document Version
Publisher's PDF, also known as Version of record

[Link back to DTU Orbit](#)

Citation (APA):
Tidemand, K. D., Christensen, H. E. M., Hoeck, N., Harris, P., Boesen, J., & Peters, G. H. J. (2016). Stabilization of Tryptophan Hydroxylase 2 by L-Phenylalanine Induced Dimerization. *F E B S Open Bio*, 6(10), 987-999. <https://doi.org/10.1002/2211-5463.12100>

General rights

Copyright and moral rights for the publications made accessible in the public portal are retained by the authors and/or other copyright owners and it is a condition of accessing publications that users recognise and abide by the legal requirements associated with these rights.

- Users may download and print one copy of any publication from the public portal for the purpose of private study or research.
- You may not further distribute the material or use it for any profit-making activity or commercial gain
- You may freely distribute the URL identifying the publication in the public portal

If you believe that this document breaches copyright please contact us providing details, and we will remove access to the work immediately and investigate your claim.

Stabilization of tryptophan hydroxylase 2 by L-phenylalanine-induced dimerization

Kasper D. Tidemand, Hans E. M. Christensen, Niclas Hoeck, Pernille Harris, Jane Boesen and Günther H. Peters

Department of Chemistry, Technical University of Denmark, Kongens Lyngby, Denmark

Keywords

analytical size exclusion chromatography; differential scanning fluorimetry; enzyme characterization; oligomerization; protein purification

Correspondence

H. E. M. Christensen and G. H. Peters,
Department of Chemistry, Technical
University of Denmark, Kemitorvet 207,
DK-2800 Kongens Lyngby, Denmark
E-mails: hemc@kemi.dtu.dk and
ghp@kemi.dtu.dk

(Received 23 May 2016, revised 20 June
2016, accepted 29 June 2016)

doi:10.1002/2211-5463.12100

Tryptophan hydroxylase 2 (TPH2) catalyses the initial and rate-limiting step in the biosynthesis of serotonin, which is associated with a variety of disorders such as depression, obsessive compulsive disorder, and schizophrenia. Full-length TPH2 is poorly characterized due to low purification quantities caused by its inherent instability. Three truncated variants of human TPH2 (*rch*TPH2; regulatory and catalytic domain, NΔ47-*rch*TPH2; truncation of 47 residues in the N terminus of *rch*TPH2, and *ch*TPH2; catalytic domain) were expressed, purified, and examined for changes in transition temperature, inactivation rate, and oligomeric state. *ch*TPH2 displayed 14- and 11-fold higher half-lives compared to *rch*TPH2 and NΔ47-*rch*TPH2, respectively. Differential scanning calorimetry experiments demonstrated that this is caused by premature unfolding of the less stable regulatory domain. By differential scanning fluorimetry, the unfolding transitions of *rch*TPH2 and NΔ47-*rch*TPH2 are found to shift from polyphasic to apparent two-state by the addition of L-Trp or L-Phe. Analytical gel filtration revealed that *rch*TPH2 and NΔ47-*rch*TPH2 reside in a monomer–dimer equilibrium which is significantly shifted toward dimer in the presence of L-Phe. The dimerizing effect induced by L-Phe is accompanied by a stabilizing effect, which resulted in a threefold increase in half-lives of *rch*TPH2 and NΔ47-*rch*TPH2. Addition of L-Phe to the purification buffer significantly increases the purification yields, which will facilitate characterization of hTPH2.

Tryptophan hydroxylase (TPH) catalyses the rate-limiting reaction in the biosynthesis of the hormone and neurotransmitter serotonin (5-HT). TPH uses the cofactor Fe^{2+} and the cosubstrates O_2 and tetrahydrobiopterin (BH_4) to generate 5-hydroxytryptophan (5-HTP) by hydroxylation of L-tryptophan (L-Trp). 5-HTP is enzymatically converted to 5-HT by aromatic amino acid decarboxylase [1,2]. TPH exists in two

isoforms, where isoform 1 (TPH1) is mainly responsible for catalyzing the rate-limiting step in the biosynthesis of peripheral serotonin, and isoform 2 (TPH2) primarily is associated with the biosynthesis of neuronal serotonin [1]. The regulation of serotonin levels is involved in various physiological and psychiatric disorders such as irritable bowel syndrome, depression, obsessive compulsive disorder, and schizophrenia [3].

Abbreviations

5-HT, 5-hydroxytryptamin (serotonin); 5-HTP, 5-hydroxytryptophan; AAAH, aromatic amino acid hydroxylase; ACT, aspartate kinase, chorismate mutase and TyrA; BH_4 , tetrahydrobiopterin; *ch*TPH2, catalytic domain of human tryptophan hydroxylase; DSC, differential scanning calorimetry; DSF, differential scanning fluorimetry; HEPES, 4-(2-hydroxyethyl)-1-piperazineethanesulfonic acid; L-Phe, L-phenylalanine; L-Trp, L-tryptophan; MBP, maltose binding protein; PAH, phenylalanine hydroxylase; *rch*TPH2, regulatory and catalytic domains of human tryptophan hydroxylase 2; *rn*PAH, *Rattus norvegicus* phenylalanine hydroxylase; SEC, size exclusion chromatography; TH, tyrosine hydroxylase; TPH, tryptophan hydroxylase.

Of these, depression is associated with decreased levels of neuronal serotonin, whereas some gastrointestinal disorders are associated with increased peripheral serotonin levels [4–6]. The serotonergic systems are therefore important targets in treatment of these disorders [7], which makes both TPH isoforms important enzymes to characterize.

Along with phenylalanine hydroxylase (PAH) and tyrosine hydroxylase (TH), TPH forms an enzyme subfamily of iron(II)-containing mono-oxygenases collectively referred to as the aromatic amino acid hydroxylases (AAAHs). Various truncated variants of all three AAAHs have been structurally characterized [8–12]. For *h*TPH, the catalytic cores of both isoforms have been structurally and enzymatically characterized [13–15] due to successful purification strategies [16,17].

All enzymes in the AAAH family form tetramers through dimers of dimers [18]. Each monomeric subunit consists of an N-terminal regulatory domain, a highly conserved catalytic domain, and a C-terminal tetramerization domain [19]. The N-terminal domains of PAH and TH contain a characteristic ACT fold motif [12,20]. From sequence analysis, TPH has also been proposed to contain an ACT domain [21]. Truncations of the regulatory domains have been found not to change the tetrameric assembly of TPH1 or TPH2 [1,22]. In contrast, when the C-terminal tetramerization domain is also removed, monomeric species are observed [1]. Deletions from the C-terminal domain of rabbit TPH1 have been demonstrated to change the macromolecular structure from a tetramer to predominantly monomeric form without compromising catalytic activity [23,24].

The available crystal structures of TPH1 only comprise the catalytic domain, while the crystal structure of TPH2 includes both the catalytic and the tetramerization domains [13,14,25–27]. The lack of structural information of the regulatory domain is partly due to the great instability of full-length TPH [16,28]. In TPH, the regulatory domain, in particular, has been found to cause instability and therefore limiting the quantities purified from *Escherichia coli* expression systems [1,16]. The regulatory domain of TPH2 has an additional 46 residues compared to TPH1, which are partly responsible for the limited purification quantities [29]. The fundamental role of the regulatory domain and the additional residues in the terminus is, however, poorly understood, as characterization is hampered by the limited purification yields. Therefore, structural insight is obtained from the crystal structure of rat phenylalanine hydroxylase (*rn*PAH) (PDB ID: 1PHZ – Clustal Omega: 35% sequence identity in the regulatory domain and 57% total sequence identity)

which comprises the catalytic and the regulatory domains. This structure lacks interpretable electron density in the first 18 residues of the N terminus, suggesting that this region is flexible [20]. The flexibility of the N terminus has also been confirmed by an NMR study [30]. By alignment of the sequences of *rn*PAH and *h*TPH2 (Fig. S1), it is found that residues 20 to 47 of *h*TPH2 align with the mobile 18 residues of *rn*PAH, which suggests that these residues of *h*TPH2 are mobile and might cause instability and insolubility. Therefore, an NΔ47-*rch*TPH2 variant was expressed, purified, and characterized.

The current study sheds light on the influence of the regulatory domain on macromolecular structure and stability of TPH2 by characterizing three truncated variants (sequences shown in Supporting information); *ch*TPH2 (catalytic domain), *rch*TPH2 (regulatory and catalytic domains), and NΔ47-*rch*TPH2 (47 residue truncation in the N-terminal domain). The tetramerization domain (residue 460–490) was removed to investigate the role of the regulatory domain when TPH2 was not in a tetramer. As TPH2 is poorly characterized due to low stability, additional efforts were made to identify ligands that could increase the stability, and hence purification yield, of TPH2.

Results and Discussion

Differential scanning fluorimetry

Very little is known about the regulation and structure of TPH as purification of this enzyme results in limited quantities. The presence of the regulatory domain is known to cause low stability and solubility [1]. To overcome this problem, substrates for the AAAH family (L-phenylalanine, L-tryptophan, and L-tyrosine), other ligands known to bind certain ACT domains (L-valine [31] and L-serine [32]), as well as D-phenylalanine, 5-HTP, and 5-HT were assayed for changes in the thermal unfolding of the TPH2 variants. The ligands were screened in a broad concentration range (0.1 μM–10 mM). For *ch*TPH2, an almost ideal two-state unfolding behavior was observed, Fig. 1. All ligands, except 5-HTP and 5-HT, were found to have no significant effect on the unfolding or T_m value of *ch*TPH2, Fig. 1. 5-HTP and 5-HT appear to change the unfolding of *ch*TPH2 from two-state to continuous; hence, no T_m values could be obtained at high ligand concentration.

Containing the regulatory domain, *rch*TPH2, gave rise to inconsistent and polyphasic unfolding curves from which no T_m values could be obtained (Fig. S2). The ligand screen showed that L-Trp and L-Phe induced

Fig. 1. Baseline corrected differential scanning fluorimetry (DSF)–ligand screen on *chTPH2* (enzyme concentration of 1 μM). Representative examples of the highest concentration of the ligands in the screen (1.5 mM for tyrosine and 10 mM for all other ligands). To the right T_m values ($n = 3$) of *chTPH2* with the respective ligands are listed (ND, Not detectable).

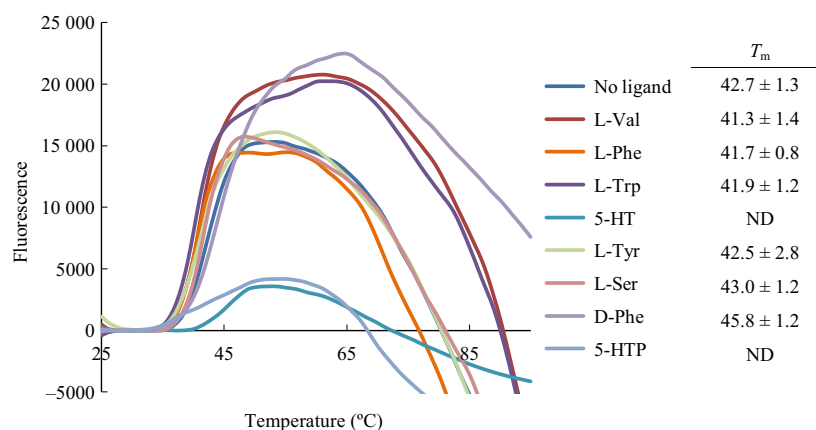
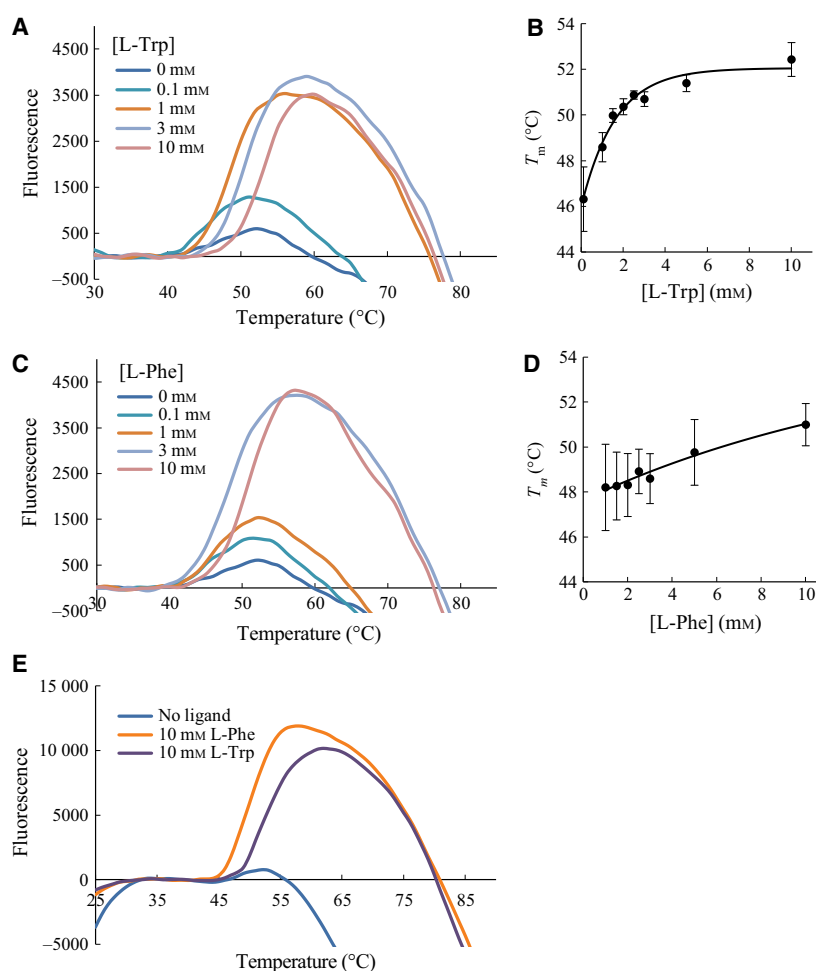


Fig. 2. Representative baseline corrected differential scanning calorimetry curves of *rchTPH2* or $\text{N}\Delta 47\text{-rchTPH2}$ (1 μM). (A) DSF curves of *rchTPH2* with different L-Trp concentration. (B) T_m values with increasing L-Trp concentration for *rchTPH2* with an exponential fit. (C) DSF curves of *rchTPH2* with different L-Phe concentration. (D) T_m values with increasing L-Phe concentration for *rchTPH2* with an exponential fit. (E) DSF of $\text{N}\Delta 47\text{-rchTPH2}$ curves in the absence of ligand, presence of 10 mM L-Phe, or presence of 10 mM L-Trp.



unfolding transitions with apparent two-state unfolding in a concentration-dependent manner (Fig. 2), which were accompanied by an increase in transition temperatures. The apparent two-state unfolding was gradually acquired with increasing ligand concentration, and robust apparent two-state unfolding was obtained at L-

Trp (Fig. 2A) and L-Phe (Fig. 2C) concentrations of 1.0 mM and 3.0 mM, respectively. At 0.1 mM L-Trp, *rchTPH2* displayed a transition temperature of 46.3 ± 1.4 $^{\circ}\text{C}$. This was increased to 52.4 ± 0.7 $^{\circ}\text{C}$ by the addition of 10.0 mM L-Trp. The exponential fit in Fig. 2B shows that saturation has been reached at

10 mM L-Trp. The transition temperature of *rch*TPH2 was increased from 48.2 ± 1.9 to 51.0 ± 0.9 °C by increasing the L-Phe concentration from 1.0 mM to 10.0 mM (Fig. 2D). Similarly, a study by Gersting *et al.* [33] utilizing differential scanning fluorimetry (DSF) found that 1 mM L-Phe increases the transition temperature of PAH from 47.5 to 50.9 °C. None of the other ligands, including D-Phe, were able to induce this change in unfolding (data not shown). The same stabilizing trend for L-Phe and L-Trp was observed for NΔ47-*rch*TPH2, Fig. 2E.

As both L-Trp and L-Phe gave rise to increased transition temperatures, a combination of the compounds was analyzed. Figure 3 shows that increasing the concentration of either L-Trp or L-Phe in the presence of the other compound results in increased T_m values, suggesting that L-Trp and L-Phe are able to increase

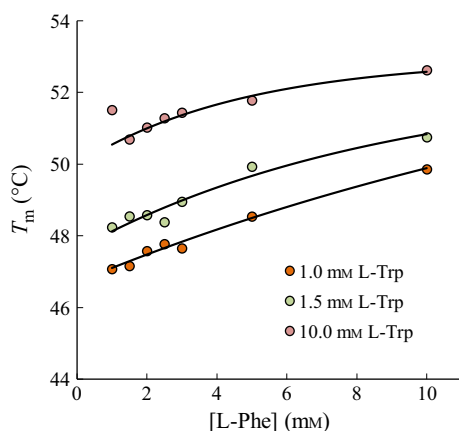


Fig. 3. Transition temperatures ($n = 3-4$) obtained from DSF experiments of *rch*TPH2 with the addition of L-Trp and L-Phe. Average standard deviation in each point is 0.8 °C. Curves represent exponential fit of T_m values as a function of [L-Phe] at constant [L-Trp]. Data for the lowest concentration of L-Phe at 10 mM L-Trp were omitted from the fit.

the transition temperature in an additive fashion. The additive effect is supported by the increase in T_m values with increasing L-Phe concentration observed at saturated concentration of L-Trp (10 mM in Fig. 3).

Analytical gel filtration

It has previously been shown in DSF assays that under stabilizing conditions multi-component complexes can change from polyphasic to almost two-state unfolding and that this is indicative of monodispersity and stability [34]. This was investigated in the case of L-Phe and L-Trp as unfolding of *rch*TPH2 and NΔ47-*rch*TPH2 was shifted toward two-state with the addition of these compounds. The oligomeric states of the TPH2 variants were analyzed utilizing analytical size exclusion chromatography (SEC). In consensus with the findings of D'Sa *et al.* [22], *ch*TPH2 was found to elute at a volume corresponding to the molecular weight of a monomer (36.2 kDa) [35]. In the loading concentration range of 2 to 60 μM, *ch*TPH2 was found only to reside as a monomer, Fig. 4. Additionally, 3 mM L-Phe did not induce any change in the elution pattern of the monodisperse solution complementing the observations from the DSF experiments.

A study by Mockus *et al.* [23] on rabbit TPH1 has demonstrated that truncation of the C-terminal tetramerization domain resulted in a disruption of the tetrameric assembly. This was also found to be the case for *h*TPH2, as SEC of NΔ47-*rch*TPH2 yielded two overlapping peaks with elution volumes corresponding to molecular weights of a monomer (47.4 kDa) and a dimer (94.9 kDa) (Fig. 5). The gradual shift of the elution peaks from a monomer to a dimer shows that NΔ47-*rch*TPH2 is found to be in a concentration-dependent monomer–dimer equilibrium. Within experimental error, the peak widths at half height were constant over the range of TPH

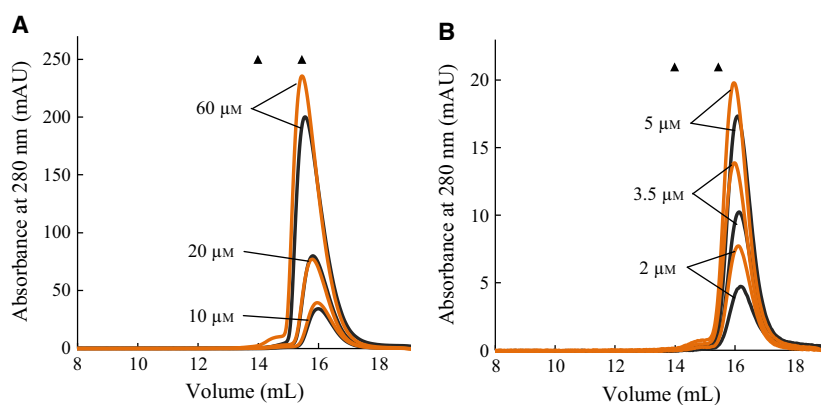


Fig. 4. Size exclusion chromatography of *ch*TPH2 with no ligand (black lines) and with the addition of 3 mM L-phenylalanine (orange lines). The markers (▲) indicate the expected elution volumes of a dimer and a monomer, respectively. Protein loading concentrations are indicated in the chromatograms. (A) High loading concentration range. (B) Low loading concentration range. AU, absorption units.

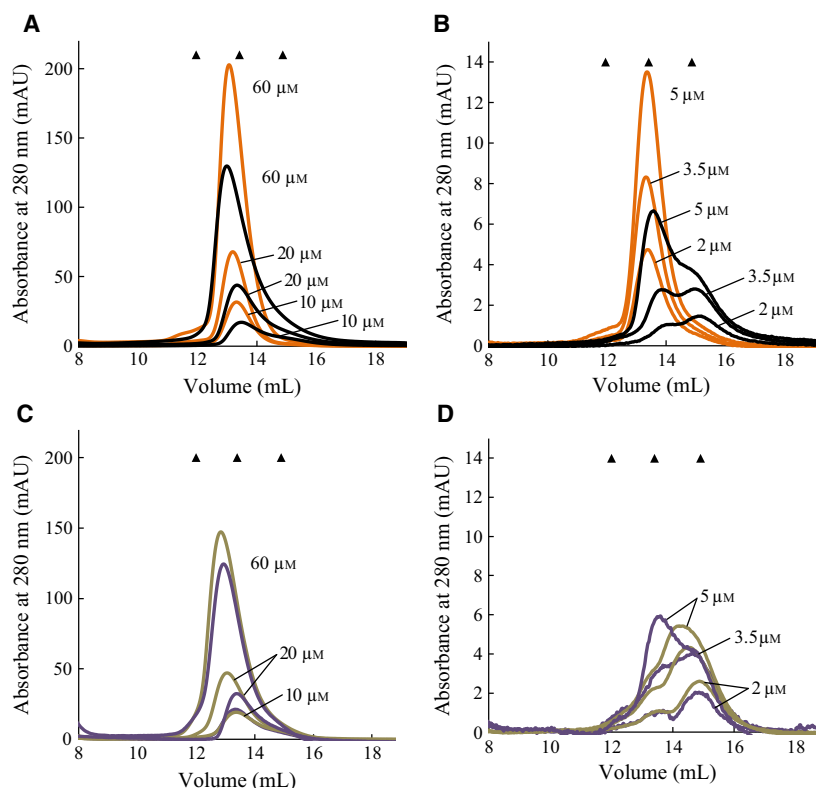


Fig. 5. Size exclusion chromatography of NΔ47-rchTPH2. (A, B) SEC without added L-Phe (black lines) and with 3 mM L-Phe (orange lines). A: High loading concentration range. B: Low loading concentration range. (C, D) SEC with the addition of 3 mM D-Phe (beige lines) or 0.5 mM L-Trp (purple lines). C: High loading concentration range. (D) Low loading concentration range. The markers (▲) indicate the expected elution volume of (from left to right) a tetramer, a dimer, and a monomer, respectively. Protein loading concentrations are indicated in the chromatograms.

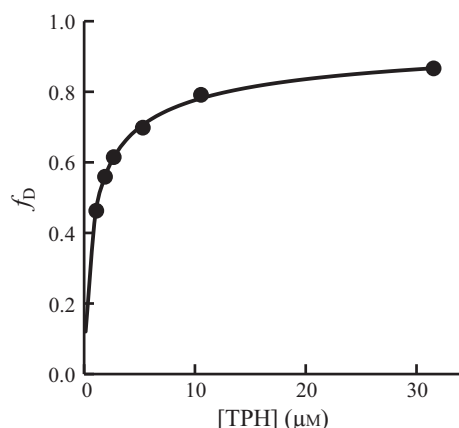


Fig. 6. Fraction of dimer as a function of NΔ47-rchTPH2 concentration (loading concentration divided by dilution factor). The solid line represents the nonlinear regression of the data using equation 11 given in Materials and methods.

concentrations, and the peak heights were also found to be related directly to the concentration of TPH injected. The dilution factor was found to be 1.90 ± 0.13 and constant within the elution range of the TPH variants. From the SEC results, the equilibrium constant, K_d , of the dissociation of a dimer into monomers was calculated (equation (7) in Materials and methods). A K_d value of $1.3 \pm 0.1 \mu\text{M}$ was found

based on the six concentrations of NΔ47-rchTPH2 in the absence of L-Phe. This value is lower than the dissociation constant of $46 \pm 35 \mu\text{M}$ determined for the dimerization of the regulatory domain of PAH [36]. A plot of fraction dimer, f_D , as a function of NΔ47-rchTPH2 concentration gave a hyperbolic-like curve as expected for a monomer–dimer equilibrium, Fig. 6.

The difference in oligomeric states of chTPH2 and rchTPH2/NΔ47-rchTPH2 shows that dimerization is caused by the regulatory domain. This finding is supported by a model structure proposed by Jiang *et al.* [37] in which the regulatory domain of one monomer forms intersubunit interactions to an adjacent monomer. The involvement of the regulatory domain in structural assembly is further supported by results from Yohrling *et al.* [38] on rabbit TPH1, where NΔ41 and NΔ90 truncations resulted in monomers indicating that the regulatory domain is involved in the formation of the tetrameric assembly. D'Sa *et al.* [22], however, found that the tetrameric assembly was retained upon truncation of the regulatory domain of human TPH2. Collectively, this might suggest that both the C-terminal tetramerization domain and the N-terminal regulatory domain contribute to the formation of a stable tetramer.

The effect of L-Phe on the monomer–dimer equilibrium was analyzed by performing SEC on

NΔ47-*rch*TPH2 samples with and without the addition of L-Phe. In Fig. 5, the black curves represent elution of NΔ47-*rch*TPH2 without the addition of L-Phe, and the orange curves represent the elution of protein when the sample and running buffer contained 3 mM L-Phe. It is evident that L-Phe shifts the equilibrium toward dimer. At a loading concentration of 2 μM NΔ47-*rch*TPH2, the addition of L-Phe was found to shift the equilibrium from predominately monomer to almost exclusively dimer. The same shift in monomer–dimer equilibrium was observed for *rch*TPH2 (Fig. 7A). This result correlates well with the observations in the DSF experiments, where the unfolding curves change from polyphasic toward two-state with the addition of L-Phe.

The influence of L-Trp and D-Phe on the monomer–dimer equilibrium was additionally analyzed to investigate the specificity of L-Phe. Figure 5C,D shows the monomer–dimer distribution of NΔ47-*rch*TPH2 with 0.5 mM L-Trp or 3 mM D-Phe in a protein concentrations range from 2 to 60 μM. From the SEC results in Fig. 5, dimerization K_d values of 1.6 ± 0.7 μM and 1.8 ± 0.9 μM were determined in the presence of L-Trp and D-Phe, respectively. 3 mM D-Phe or 0.5 mM L-Trp does, therefore, not change the monomer–dimer equilibrium constant. At a TPH2 loading concentration of 2 μM, it is evident by comparison of Fig. 5B,D that neither the addition of 0.5 mM L-Trp nor 3 mM D-Phe induced the shift in the monomer–dimer equilibrium toward dimer as observed for L-Phe. L-Trp absorption introduced high background noise and was hence only added to concentrations of 0.5 and 1.0 mM. As a consequence of the background noise, chromatograms of NΔ47-*rch*TPH2 with loading concentrations below 5 μM could not be obtained at 1.0 mM L-Trp. However, at low protein concentrations (5–20 μM), the monomer–dimer equilibrium does not seem to be influenced by 1.0 mM L-Trp as monomer is present (Fig. 7B), which is not observed in the presence of L-Phe (Fig. 5A,B). The addition of 1 mM L-Trp is

compared with 3 mM L-Phe as these concentrations were found in the DSF experiments to change the unfolding from polyphasic to apparent two-state (Fig. 2A,C). The fact that L-Trp did not induce the same shift in equilibrium suggests that the stabilization observed in the DSF experiments occurs through a different mechanism than for L-Phe. Furthermore, L-Phe binding is found to be specific as D-Phe did not induce dimerization. That L-Trp does not induce dimerization in *rch*TPH2 extends recent results obtained by Patel *et al.*, who showed that among the regulatory domains of TH, PAH, and TPH1, only PAH dimerizes in the presence of its natural substrate [39].

Thermal inactivation

To investigate if the dimerizing effect had an impact on TPH2 stability, rates of inactivation at 30 °C in the presence or absence of 3 mM L-Phe were examined. The data were fitted with one-exponential decay curves, and the rate constants, k , were calculated using an exponential function, $E_t = E_0 e^{-kt}$, where E_0 is the initial enzyme activity, and E_t is the activity after time t at 30 °C (Fig. 8). From the decay rate constants, half-lives ($t_{1/2}$) of the *h*TPH2 variants were calculated using $t_{1/2} = \ln(2)/k$. At 30 °C and a concentration of 5 μM, *rch*TPH2, and NΔ47-*rch*TPH2 displayed $t_{1/2}$ values of only 15 ± 2 and 18 ± 3 min, respectively. Hence, truncation of the N terminus slightly increased the $t_{1/2}$ value ($P = 0.18$, T -test). With a $t_{1/2}$ value of 203 ± 40 min, *ch*TPH2 displayed a 14-fold higher half-life compared to *rch*TPH2, which is in agreement with the results of Carkaci-Salli *et al.* [1] and confirms that the presence of the regulatory domain causes significant destabilization. With addition of 3 mM L-Phe, $t_{1/2}$ values of 41 ± 3 , 49 ± 5 , and 193 ± 29 min were obtained for *rch*TPH2, NΔ47-*rch*TPH2, and *ch*TPH2, respectively. Variants containing the regulatory domain displayed nearly 3-fold increase in half-lives whereas *ch*TPH2 was not significantly influenced by L-Phe.

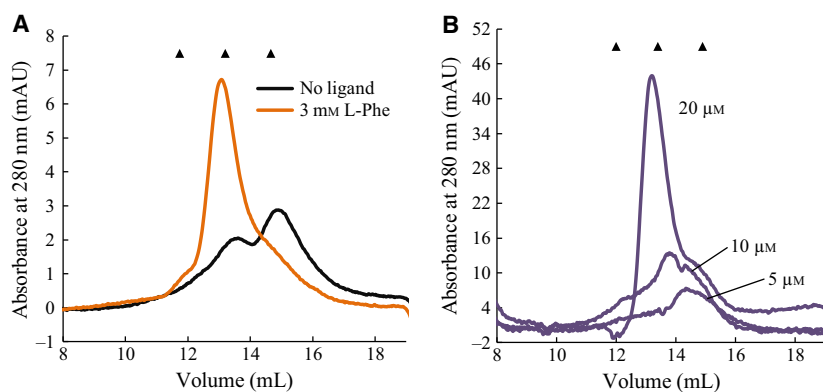


Fig. 7. (A) Size exclusion chromatography of *rch*TPH2 (loading concentration of 2 μM), with no ligand (black line) and with the addition of 3 mM L-Phe (orange line). (B) Size exclusion chromatography of NΔ47-*rch*TPH2, with the addition of 1 mM L-Trp. Protein loading concentrations are indicated in the chromatogram. The markers (▲) indicate the expected elution volumes of a tetramer, a dimer, and a monomer, respectively.

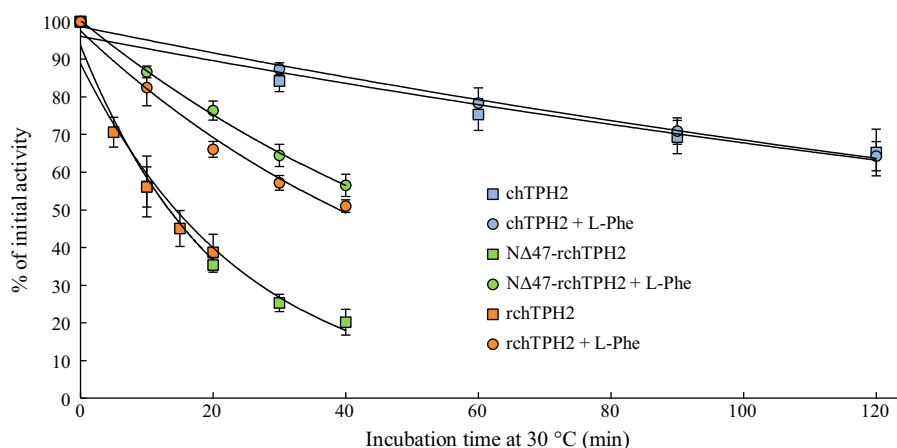


Fig. 8. Heat inactivation of hTPH2 variants. Enzyme samples (5 μ M) were incubated at 30 °C, and residual activity in % of initial activity at t_0 was assayed in time intervals. The curves are fit to the mean of three independent measurements performed on each variant. Squares and circles present heat inactivation in the absence or presence of 3 mM L-Phe, respectively.

That the stabilizing effect is exclusively observed for rchTPH2 and NΔ47-rchTPH2 implies that L-Phe is stabilizing through binding to the regulatory domain. Further, as L-Phe induces a stabilizing effect in both rchTPH2 and NΔ47-rchTPH2, binding of L-Phe does not seem to involve the 47 N-terminal residues. L-Phe induced stability and shift in equilibrium toward dimer imply that TPH2 variants containing the regulatory domain are more stable as dimers.

A stabilizing effect of L-Trp has previously been observed by McKinney *et al.* [16] who hypothesized that L-Trp might stabilize through binding in the active site, which might tighten up flexible regions, and hereby protect the active site. The increase in T_m (DSF) upon the addition of L-Phe or L-Trp might, analogously to the hypothesis of McKinney *et al.* [16], occur through binding in the active site which in turn induces a more closed conformation, as it has been seen for binding of tryptophan in chicken TPH [25]. However, a shift in the monomer–dimer equilibrium is only observed for L-Phe, suggesting that the increase in T_m and half-life occur through different mechanisms. Alternatively, L-Phe binds in an allosteric site which stabilizes the regulatory domain through improved interactions with an adjacent monomer. Such an allosteric site in the regulatory domain has been identified in PAH, which has been found to increase PAH activity and stability and induce large conformational changes [20,39–41]. This is consistent with the binding of amino acids to ACT domains which often occurs at domain interfaces and results in conformational changes [42]. This hypothesis is supported by the observed shift in monomer–dimer equilibrium and the additive effect of L-Trp and L-Phe

observed in the DSF experiments. Such an allosteric site might have relevance *in vivo* functioning as an allosteric modulating site that stabilizes a dimer in the native tetramer (dimer of dimers). Stabilization of the tetramer is important as disruption of the native tetramer results in decreased enzymatic activity [43].

Differential scanning calorimetry

The transition temperatures, T_m , of the TPH2 variants were measured utilizing differential scanning calorimetry (DSC), to investigate if the low half-life of rchTPH2 is caused by premature unfolding of the regulatory domain. The DSC experiments were performed in the presence of L-Phe to observe domain unfolding in a monodisperse solution. All variants displayed irreversible unfolding upon reheating and hence, only T_m values were extracted from the thermograms. Illustrative examples of DSC thermograms of the three variants are presented in Fig. 9.

The unfolding transitions of the three variants seem equivalent, however, by comparison of the thermograms of chTPH2 and NΔ47-rchTPH2 (Fig. 9A,B), it is evident that truncation of the regulatory domain resulted in a reduction in the heat capacity of the low temperature transition ($T_{m(\text{low})}$). This suggests that the lowest temperature transitions are partly due to the unfolding of the regulatory domain, as suggested for hPAH by Thórolfsson *et al.* [44]. The remaining transitions, therefore, originate from the unfolding of the more stable catalytic domain, quantified by the transition temperature of the main peak in the thermograms ($T_{m(\text{high})}$). Transition temperatures obtained from the thermograms are presented in Table 1.

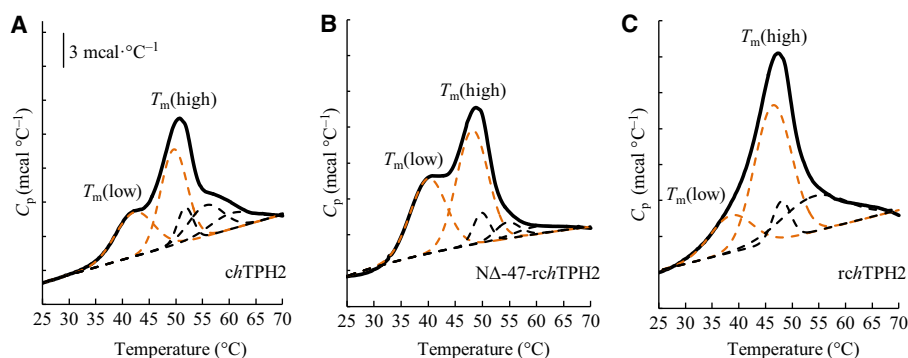


Fig. 9. Examples of DSC thermograms of *chTPH2* (A), *NΔ47-rchTPH2* (B), and *rcTPH2* (C) purified in L-Phe buffer. All variants were analyzed at a concentration of 35 μM . DSC data after baseline subtraction are shown in solid lines and individual peaks from deconvolution as dashed lines. The quantified transitions marked $T_m(\text{low})$ and $T_m(\text{high})$ are highlighted in orange dashed lines.

Table 1. The transition temperature of the investigated *hTPH2* variants obtained from DSC, where means \pm SD of $T_m(\text{low})$ and $T_m(\text{high})$ values (Fig. 9) obtained from three independent experiments are listed. A protein concentration of 35 μM was used in all measurements.

	<i>rcTPH2</i>	<i>NΔ47-rchTPH2</i>	<i>chTPH2</i>
$T_m(\text{low})$, $^{\circ}\text{C}$	40.1 ± 1.2	39.6 ± 0.5	41.7 ± 0.4
$T_m(\text{high})$, $^{\circ}\text{C}$	46.8 ± 0.3	47.7 ± 0.5	49.7 ± 0.1

Deletion of the regulatory domain increased the T_m values of the two main transitions by 1.6 and 2.9 $^{\circ}\text{C}$, respectively. Truncation of the N terminus only induced a slight increase in the $T_m(\text{high})$ value ($P = 0.053$, T -test).

The regulatory and catalytic domains of *rcTPH2* unfold at 40.1 ± 1.2 $^{\circ}\text{C}$ and 46.8 ± 0.3 $^{\circ}\text{C}$, respectively. These results are, despite variations in the buffer systems, in the same range as previously reported transition temperatures for AAHs (47.5–55.5 $^{\circ}\text{C}$) [33,45,46]. The DSC data relate to the inactivation measurements, as unfolding of the variants containing the regulatory domain is initiated at around 30 $^{\circ}\text{C}$ (Fig. 9C,B), which is the temperature of the inactivation measurements, and around 35 $^{\circ}\text{C}$ for *chTPH2* (Fig. 9A). This might explain the significantly higher $t_{1/2}$ values observed for *chTPH2* at 30 $^{\circ}\text{C}$. Unfolding of *rcTPH2* shows a less profound low temperature transition compared to *NΔ47-rchTPH2*. This might be explained by the mobile N terminus causing a less defined regulatory domain which seems to unfold more continuously initiated at lower temperature than observed for *chTPH2*. Furthermore, the presence of the regulatory domain causes an earlier unfolding of the catalytic domain; this signifies that attempts to stabilize TPH should occur through the regulatory domain.

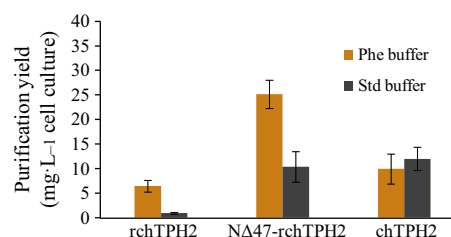


Fig. 10. Purification yields ($\text{mg}\cdot\text{L}^{-1}$ cell culture, $n = 2\text{--}6$) of the three *hTPH2* variants (mean \pm SD). Orange and dark gray bars state yields obtained from purifications using Phe buffer (20 mM HEPES/ NH_4OH , 300 mM $(\text{NH}_4)_2\text{SO}_4$, pH 7.0, and 3 mM L-Phe) and Std buffer (20 mM HEPES/ NH_4OH , 300 mM $(\text{NH}_4)_2\text{SO}_4$, and pH 7.0), respectively.

Purification yield

Characterization of *hTPH2* variants containing the regulatory domain has been hampered by the low quantities obtained from *E. coli*, partially due to the poor stability. Figure 10 presents the purification yields obtained for the three variants with and without L-Phe added to the purification buffer. Without L-Phe, very low purification quantities were obtained for *rcTPH2* (0.9 ± 0.2 $\text{mg}\cdot\text{L}^{-1}$) compared to *chTPH2* (12.0 ± 2.4 $\text{mg}\cdot\text{L}^{-1}$). The low quantities for *rcTPH2* were overcome by truncation of the N terminus which resulted in an 11-fold increase in yield (10.4 ± 3.1 $\text{mg}\cdot\text{L}^{-1}$), which was similar to that of *chTPH2*.

The stabilizing effect of L-Phe was reflected in the purification yields, as they were increased seven- and twofold for *rcTPH2* (6.4 ± 1.2 $\text{mg}\cdot\text{L}^{-1}$) and *NΔ47-rchTPH2* (25.1 ± 2.9 $\text{mg}\cdot\text{L}^{-1}$), respectively (Fig. 10). In line with the results observed in the inactivation experiment, no significant change in purification yield was observed for *chTPH2* (9.9 ± 3.1 $\text{mg}\cdot\text{L}^{-1}$).

Conclusion

The current results demonstrate that L-Trp and L-Phe change the unfolding mechanism of *h*TPH2, but only when the regulatory domain is present. Deletion of the C-terminal tetramerization domain results in a monomer–dimer equilibrium which is shifted to predominately dimer with the addition of L-Phe. In the presence of L-Phe, the dimer displayed significantly increased half-life which in turn resulted in significantly increased purification yields of *h*TPH2 variants containing the regulatory domain. These findings will facilitate future characterization of *h*TPH2.

Materials and methods

Materials

All used chemicals were of analytical grade, and all solutions were prepared using water from an 18.2 M Ω -cm Milli-Q synthesis A10 Q-Gard system which was filtered through a 0.22- μ m filter. Protein purification was performed on an ÄKTA purifier 100 from GE Healthcare. Utilized GE Healthcare column variants: HiLoad Superdex 200 26/60 pg, Superdex 200 10/300 GL, and a XK 16/20 column packed with 25 mL Dextrin Sepharose High Performance media. During purifications, all TPH-containing solutions were kept in ice water, except during the chromatographic steps, which were performed at room temperature. Protein solutions were concentrated using an Amicon ultrafiltration cell with an Ultracell PL-3 membrane. Protein concentrations were determined by measuring the absorbance at 280 nm on an ND-1000 NanoDrop Spectrophotometer from Saveen Werner (Limhamn, Sweden).

Cloning and expression

Full-length human TPH2 cDNA optimized for expression in *E. coli* was obtained from GenScript (Piscataway, NJ, USA). All proteins were expressed as maltose binding protein fusion proteins from the pET26 expression vector in *E. coli* BL21 (DE3) (Novagen, Merck Millipore, Darmstadt, Germany) cells. The sequences of the proteins expressed are given in the Supporting information. The recombinant fusion proteins contain a cleavage recognition site for human rhinovirus 3C protease (3CP) [47]. The construct encoding the different protein variants was obtained by PCR. The primers used are listed in Table S1. All DNA sequences were verified by sequencing (Eurofins). Proteins were expressed at 20 °C for 14 h, as previously described [17]. MBP-3CP was cloned and expressed in-house in a similar manner.

Purification

Escherichia coli cells from 650 mL cultures were thawed from –80 °C and resuspended in buffer containing 20 mM

HEPES/NH₄OH, 300 mM (NH₄)₂SO₄, pH 7.0 (standard buffer, Std buffer) or 20 mM HEPES/NH₄OH, 300 mM (NH₄)₂SO₄, pH 7.0, and 3 mM L-Phe (Phe buffer), to a volume of 40 mL. (NH₄)₂SO₄ was included in the purification buffer, as it has been found that the purification yield of recombinant catalytic core of rabbit TPH1 was enhanced by the addition of ammonium sulfate [24]. The resuspended cell culture was lysed by sonication for 3 \times 30 s using a Satorius Labsonic at 80% amplitude, while kept in ice water. The lysed sample was centrifuged at 4 °C and 18 000 g for 20 min. The supernatant was decanted to another tube and centrifuged a second time at 4 °C and 18 000 g for 20 min, while the pellet was discarded. The supernatant was collected and filtered through a 0.45- μ m filter. A volume of approximately 35 mL filtered supernatant was loaded with a flow rate of 5 mL \cdot min^{–1} onto a Dextrin Sepharose column, which was equilibrated with five column volumes of Std or Phe buffer. Following sample loading, an MBP-3CP solution was prepared by diluting MBP-3CP from stock with Std or Phe buffer to a concentration of 2.2 μ M. About 30-mL MBP-3CP solution was loaded onto the column with a flow rate of 5 mL \cdot min^{–1}, and the column was incubated at room temperature for 1 h. Once the flow (5 mL \cdot min^{–1}) was resumed, 10 mL of the protein-containing eluate was collected. The collected solution, containing target protein, was filtered through a 0.45- μ m filter prior to loading on a HiLoad Superdex 200 prep grade column, which had been equilibrated with two column volumes of Std or Phe buffer. Std or Phe buffer was used as mobile phase using a flow rate of 2.5 mL \cdot min^{–1}, and UV-detected (280 nm) peaks containing the target protein (verified by SDS/PAGE analysis – Figs S3–S5) were collected. The concentration of the collected protein was determined by UV-Vis absorption at 280 nm utilizing theoretical extinction coefficients obtained from ExPASy [48]. The samples were either concentrated by ultrafiltration prior to freezing in liquid nitrogen, or if the concentration of target protein was high enough in the eluate, the ultrafiltration was bypassed, and the protein solution was frozen in liquid nitrogen and stored at –80 °C.

SDS/PAGE

Evaluation of molecular weights and purity were conducted by SDS/PAGE. Proteins were resolved on Mini-PROTEAN TGX gels (7.5%) from Bio-Rad (Hercules, CA, USA) run at 100 V for 75 min with a protein standard from Bio-Rad (no. 161-0304). Gels were stained with Coomassie Blue to visualize the proteins.

Differential scanning fluorimetry

The unfolding of the TPH2 variants was recorded with an Agilent Technologies Stratagene MX3005 P RT-PCR machine (Santa Clara, CA, USA). The ligand screen was

performed with a total volume of 25 μL in 96-well plates (polypropylene plates from Agilent Technologies). Each well was composed of protein at a concentration of 1 μM , SYPRO orange at a concentration of $2\times$ (diluted from SYPRO[®] 5000 \times stock from Sigma, St. Louis, MO, USA), and ligand (diluted in purification buffer) in a concentration range of 0.1 μM to 10 mM. Each plate contained control wells with the purification buffer with and without protein and ligand. Scans were carried out using a scan rate of 1 $^{\circ}\text{C}\cdot\text{min}^{-1}$, going from 20 $^{\circ}\text{C}$ to 95 $^{\circ}\text{C}$. The thermograms were baseline corrected with MXPRO QPCR Software (Agilent Technologies, Santa Clara, CA, USA) and analyzed for transition temperatures with GRAPH PAD PRISM 6 (GraphPad Software, Inc, La Jolla, CA, USA) utilizing a Boltzmann sigmoid fit:

$$y = \text{LL} + \frac{\text{UL} - \text{LL}}{1 + \exp\left(\frac{T_m - x}{a}\right)}$$

where LL and UL are the values of minimum and maximum intensities, respectively, and a denotes the slope of the unfolding curve at T_m [49].

Analytical size exclusion chromatography

Determination of the oligomeric state of the TPH2 variants was performed on a Superdex 200 10/300 GL column. Prior to analysis, the column was equilibrated with two column volumes of the buffer of investigation, and the samples were spiked with concentrated stock solutions of L-Trp, L-Phe, or D-Phe and allowed to equilibrate for 20 min. Samples were injected with a 500 μL loop and analyzed at a flow rate of 0.5 $\text{mL}\cdot\text{min}^{-1}$. Calibration curve of molecular weights was obtained from GE Healthcare [35].

The equilibrium constant of the dissociation of a dimer into monomers was based on the scheme below



The equilibrium dissociation constant, K_d , is defined by

$$K_d = \frac{[\text{M}]^2}{[\text{D}]} \quad (1)$$

where $[\text{M}]$ and $[\text{D}]$ are the molar concentrations of monomer and dimer, respectively. The total protein concentration, $[\text{M}]_{\text{total}}$, can be expressed in terms of molar monomer equivalents

$$[\text{M}]_{\text{total}} = [\text{M}] + 2[\text{D}] \quad (2)$$

and the concentration of dimer is therefore given by

$$[\text{D}] = \frac{[\text{M}]_{\text{total}} - [\text{M}]}{2} \quad (3)$$

Under the assumptions that $\varepsilon_{280,\text{dimer}} = 2 \cdot \varepsilon_{280,\text{monomer}}$ and area under the size exclusion curve (SEC) curve (AUC) \propto $[\text{M}]$, the molecular concentration of monomer is given by

$$[\text{M}] = \frac{\text{AUC}_M}{\text{AUC}_M + \text{AUC}_D} * [\text{M}]_{\text{total}} \quad (4)$$

where AUC_M and AUC_D are the area under the curve of the peaks representing the monomer and dimer, respectively, obtained by deconvolution of the chromatograms from the SEC experiments. Substituting $[\text{M}]$ in equation (3) by the expression of $[\text{M}]$ in equation (4) yields

$$[\text{D}] = \frac{1}{2} \frac{\text{AUC}_D}{\text{AUC}_M + \text{AUC}_D} [\text{M}]_{\text{total}} \quad (5)$$

where $\text{AUC}_D/(\text{AUC}_M + \text{AUC}_D)$ is the mole fraction of dimer, f_D . Substituting $[\text{M}]$ and $[\text{D}]$ from equation (4) and (5), respectively, into equation (1) yields

$$K_d = \frac{2 * \text{AUC}_M^2 * [\text{M}]_{\text{total}}}{\text{AUC}_D * (\text{AUC}_D + \text{AUC}_M)} \quad (6)$$

The sample concentration loaded in SEC will be diluted during separation. Therefore, when applying equation (6), $[\text{M}]_{\text{total}}$ must be divided by the dilution factor, DF, introduced during gel filtration

$$K_d = \frac{2 * \text{AUC}_M^2 * \frac{[\text{M}]_{\text{total}}}{\text{DF}}}{\text{AUC}_D * (\text{AUC}_D + \text{AUC}_M)} \quad (7)$$

The dilution factor during elution was measured by the width at half height of the peak divided by the sample load volume [50]. This was performed only on monodisperse solutions. The fraction of dimer, f_D , as a function of $[\text{M}]_{\text{total}}$ can be expressed as

$$[\text{D}] = \frac{1}{2} * f_D * \frac{[\text{M}]_{\text{total}}}{\text{DF}} \quad (8)$$

$$[\text{M}] = (1 - f_D) * \frac{[\text{M}]_{\text{total}}}{\text{DF}} \quad (9)$$

Substituting $[\text{M}]$ and $[\text{D}]$ from equation (8) and (9), respectively, into equation (1) yields

$$K_d = \frac{\left((1 - f_D) * \frac{[\text{M}]_{\text{total}}}{\text{DF}} \right)^2}{f_D * \frac{1}{2} * \frac{[\text{M}]_{\text{total}}}{\text{DF}}} \quad (10)$$

Solving equation (10) for the fraction of dimer, f_D , yields

$$f_D = \frac{\frac{1}{4} \left(4 * \frac{[\text{M}]_{\text{total}}}{\text{DF}} + K_d - 1 * \sqrt{K_d^2 + 8 * K_d * \frac{[\text{M}]_{\text{total}}}{\text{DF}}} \right)}{\frac{[\text{M}]_{\text{total}}}{\text{DF}}} \quad (11)$$

Activity assay

The activity measurements were performed using a Varian Cary Eclipse Fluorescence Spectrophotometer. For activity measurements, the *h*TPH2 variants were thawed under running water, filtered, and the concentrations were

determined by UV-Vis absorption at 280 nm. The hTPH2 samples were diluted to a protein concentration of 5 μM in the buffer in which it was purified. TPH2 activity was assayed in a reaction mixture (10 \times 10 mm QS quartz cuvette from Hellma (Müllheim, Germany) – 2500 μL total volume) containing 50 mM HEPES/ NH_4OH , 200 mM $(\text{NH}_4)_2\text{SO}_4$, pH 7.0, 0.025 $\text{g}\cdot\text{L}^{-1}$ catalase, 25 μM $(\text{NH}_4)_2\text{Fe}(\text{II})(\text{SO}_4)_2\cdot 6\text{H}_2\text{O}$, 7 mM dithiothreitol (DTT), 60 μM L-Trp, and 300 μM BH_4 with stirring at 15 $^\circ\text{C}$ [14,51]. The excitation wavelength was 300 nm, and the emission was monitored at 330 nm. The activities were determined by the initial slope (intensity $\cdot\text{min}^{-1}$) of the monitored fluorescence and were quantified using VARIAN SPECTROPHOTOMETER software (Agilent Technologies). Quantification occurred through linear regression on a manually placed interval of minimum 0.04 min of the initial curve. Denaturation was performed by heating the protein in aliquots of 1300 μL to 30 $^\circ\text{C}$ in a water bath. The denaturation was stopped by cooling the protein solution in ice water.

Differential scanning calorimetry

Differential scanning calorimetry (DSC) measurements were carried out on a TA Instruments (New Castle, DE, USA) 6300 Nano DSC. Solutions of protein in L-Phe containing buffer were used for sample measurements, and the same buffer as used in the purification of the hTPH2 variants were used as references. Prior to sample loading, the protein sample and the reference buffer were degassed at approximately 10 $^\circ\text{C}$ using a MicroCal (MicroCal, LLC, Northhampton, MA, USA) USB ThermoVac. Three hundred microliters of protein sample and reference buffer were loaded in the respective cells. A constant pressure of 3 atm was applied, and scans were carried out using a scan rate of 1 $^\circ\text{C}\cdot\text{min}^{-1}$, going from 5 $^\circ\text{C}$ to 70 $^\circ\text{C}$. Deconvolution of the thermograms was performed with Peakfit v4.12 using Gaussian peak functions.

Acknowledgements

KDT acknowledges financial support via an Academic Excellence Scholarship from the Department of Chemistry, Technical University of Denmark. The authors would like to thank Esben Thormann and Jonas R. Henriksen for providing access to their differential scanning calorimeter, as well as David F. Nielsen and Martin H. Pedersen for technical assistance.

Author contributions

KDT: Wrote the paper, performed experiments, and analyzed the data. HEMC and GHP: Designed experiments, contributed to data analysis and in writing the

paper. NH and JB: Performed preliminary experiments. PH: Contributed to writing the paper.

References

- 1 Carkaci-Salli N, Flanagan JM, Martz MK, Salli U, Walther DJ, Bader M and Vrana KE (2006) Functional domains of human tryptophan hydroxylase 2 (hTPH2). *J Biol Chem* **281**, 28105–28112.
- 2 Udenfriend S, Clark CT and Titus E (1953) 5-hydroxytryptophan decarboxylase: a new route of metabolism of tryptophan. *J Am Chem Soc* **75**, 501–502.
- 3 Costagliola C, Parmeggiani F, Semeraro F and Sebastiani A (2008) Selective serotonin reuptake inhibitors: a review of its effects on intraocular pressure. *Curr Neuropharmacol* **6**, 293–310.
- 4 Liu Q, Yang Q, Sun W, Vogel P, Heydorn W, Yu X, Hu Z, Yu W, Jonas B, Pineda R *et al.* (2008) Discovery and characterization of novel tryptophan hydroxylase inhibitors that selectively inhibit serotonin synthesis in the gastrointestinal tract. *J Pharmacol Exp Ther* **325**, 47–55.
- 5 Popova NK and Kulikov AV (2010) Targeting tryptophan hydroxylase 2 in affective disorder. *Expert Opin Ther Targets* **14**, 1259–1271.
- 6 Matthes S, Mosienko V, Bashammakh S, Alenina N and Bader M (2010) Tryptophan hydroxylase as novel target for the treatment of depressive disorders. *Pharmacology* **85**, 95–109.
- 7 Torrente MP, Gelenberg AJ and Vrana KE (2012) Boosting serotonin in the brain: is it time to revamp the treatment of depression? *J Psychopharmacol* **26**, 629–635.
- 8 Andersen OA, Flatmark T and Hough E (2001) High resolution crystal structures of the catalytic domain of human phenylalanine hydroxylase in its catalytically active Fe(II) form and binary complex with tetrahydrobiopterin. *J Mol Biol* **314**, 279–291.
- 9 Erlandsen H, Fusetti F, Martinez A, Hough E, Flatmark T and Stevens RC (1997) Crystal structure of the catalytic domain of human phenylalanine hydroxylase reveals the structural basis for phenylketonuria. *Nat Struct Biol* **4**, 995–1000.
- 10 Andersen OA, Stokka AJ, Flatmark T and Hough E (2003) 2.0 Å resolution crystal structure of the ternary complex of human phenylalanine hydroxylase with tetrahydrobiopterin and 3-(2-thienyl)-L-alanine, or L-norleucine: substrate specificity and molecular motions related to substrate binding. *J Mol Biol* **333**, 747–757.
- 11 Goodwill KE, Sabatier C, Marks C, Raag R, Fitzpatrick PF and Stevens RC (1997) Crystal structure of tyrosine hydroxylase at 2.3 Å and its implications for inherited neurodegenerative diseases. *Nat Struct Biol* **4**, 578–585.

- 12 Zhang S, Huang T, Ilangoan U, Hinck AP and Fitzpatrick PF (2014) The solution structure of the regulatory domain of tyrosine hydroxylase. *J Mol Biol* **426**, 1483–1497.
- 13 Wang L, Erlandsen H, Haavik J, Knappskog PM and Stevens RC (2002) Three-dimensional structure of human tryptophan hydroxylase and its implications for the biosynthesis of the neurotransmitters serotonin and melatonin. *Biochemistry* **41**, 12569–12574.
- 14 Kopeck J, Oberholzer A, Fitzpatrick PF, Newman J, Tallant C, Kiyani W, Shrestha L, Burgess-Brown N, von Delft F, Arrowsmith C *et al.* (2014) Crystal structure of human tryptophan hydroxylase 2 (TPH2), catalytic domain, pdb entry: 4V06.
- 15 Windahl MS, Boesen J, Karlsen PE and Christensen HEM (2009) Expression, purification and enzymatic characterization of the catalytic domains of human tryptophan hydroxylase isoforms. *Protein J* **28**, 400–406.
- 16 McKinney J, Knappskog PM, Pereira J, Ekern T, Toska K, Kuitert BB, Levine D, Gronenborn AM, Martinez A and Haavik J (2004) Expression and purification of human tryptophan hydroxylase from *Escherichia coli* and *Pichia pastoris*. *Protein Expr Purif* **33**, 185–194.
- 17 Nielsen MS, Petersen CR, Munch A, Vendelboe TV, Boesen J, Harris P and Christensen HEM (2008) A simple two step procedure for purification of the catalytic domain of chicken tryptophan hydroxylase 1 in a form suitable for crystallization. *Protein Expr Purif* **57**, 116–126.
- 18 Liberles JS, Thóroldsson M and Martínez A (2005) Allosteric mechanisms in ACT domain containing enzymes involved in amino acid metabolism. *Amino Acids* **28**, 1–12.
- 19 Fitzpatrick PF (1999) Tetrahydropterin-dependant amino acid hydroxylases. *Annu Rev Biochem* **68**, 355–381.
- 20 Kobe B, Jennings IG, House CM, Michell BJ, Goodwill KE, Santarsiero BD, Stevens RC, Cotton RG and Kemp BE (1999) Structural basis of autoregulation of phenylalanine hydroxylase. *Nat Struct Biol* **6**, 442–448.
- 21 Aravind L and Koonin EV (1999) Gleaning non-trivial structural, functional and evolutionary information about proteins by iterative database searches. *J Mol Biol* **287**, 1023–1040.
- 22 D'Sa CM, Arthur RE and Kuhn DM (1996) Expression and deletion mutagenesis of tryptophan hydroxylase fusion proteins: delineation of the enzyme catalytic core. *J Neurochem* **67**, 917–926.
- 23 Mockus SM, Kumer SC and Verana KE (1997) Carboxyl terminal deletion analysis of tryptophan hydroxylase. *Biochim Biophys Acta* **1342**, 132–140.
- 24 Moran GR, Daubner SC and Fitzpatrick PF (1998) Expression and characterization of the catalytic core of tryptophan hydroxylase. *J Biol Chem* **273**, 12259–12266.
- 25 Windahl MS, Petersen CR, Christensen HEM and Harris P (2008) Crystal structure of tryptophan hydroxylase with bound amino acid substrate. *Biochemistry* **47**, 12087–12094.
- 26 Jin H, Cianchetta G, Devasagayaram A, Gu K, Marinelli B, Samala L, Scott S, Stouch T, Tunoori A, Wang Y *et al.* (2009) Substituted 3-(4-(1,3,5-triazin-2-yl)-phenyl)-2-aminopropanoic acids as novel tryptophan hydroxylase inhibitors. *Bioorg Med Chem Lett* **19**, 5229–5232.
- 27 Cianchetta G, Stouch T, Yu W, Shi Z, Tari LW, Swanson RV, Hunter MJ, Hoffman ID and Liu Q (2010) Mechanism of inhibition of novel tryptophan hydroxylase inhibitors revealed by co-crystal structures and kinetic analysis. *Curr Chem Genomics* **4**, 19–26.
- 28 D'Sa CM, Arthur Jr RE, States JC and Kuhn DM (1996) Tryptophan hydroxylase: cloning and expression of the rat brain enzyme in mammalian cells. *J Neurochem* **67**, 900–906.
- 29 Murphy KL, Zhang X, Gainetdinov RR, Beaulieu JM and Caron MG (2008) A regulatory domain in the N-terminus of tryptophan hydroxylase 2 controls enzyme expression. *J Biol Chem* **283**, 13216–13224.
- 30 Horne J, Jennings IG, Teh T, Gooley PR and Kobe B (2002) Structural characterization of the N-terminal autoregulatory sequence of phenylalanine hydroxylase. *Protein Sci* **11**, 2041–2047.
- 31 Chen L, Chen Z, Zheng P, Sun J and Zeng AP (2012) Study and reengineering of the binding sites and allosteric regulation of biosynthetic threonine deaminase by isoleucine and valine in *Escherichia coli*. *Appl Microbiol Biotechnol* **97**, 2939–2949.
- 32 Schuller DJ, Grant GA and Banaszak LJ (1995) The allosteric ligand site in the V-max-Type cooperative enzyme phosphoglycerate dehydrogenase. *Nat Struct Biol* **2**, 69–76.
- 33 Gersting SW, Staudigl M, Truger MS, Messing DD, Danecka MK, Sommerhoff CP, Kemter KF and Muntau AC (2010) Activation of phenylalanine hydroxylase induces positive cooperativity towards the natural cofactor. *J Biol Chem* **285**, 30686–30697.
- 34 Chari A, Haselbach D, Kirves JM, Ohmer J, Paknia E, Fischer N, Ganichkin O, Möller V, Frye JJ, Petzold G *et al.* (2015) ProteoPlex: stability optimization of macromolecular complexes by sparse-matrix screening of chemical space. *Nat Methods* **12**, 859–865.
- 35 Calibration curve obtained from: GE Healthcare, Gel Filtration Calibration Kit LMW, Gel Filtration Kit HMW, Data File 28-4073-84-AA.
- 36 Zhang S, Roberts KM and Fitzpatrick PF (2014) Phenylalanine binding is linked to dimerization of the

- regulatory domain of phenylalanine hydroxylase. *Biochemistry* **53**, 6625–6627.
- 37 Jiang GC, Yohrling GJ, Schmitt JD and Vrana KE (2000) Identification of substrate orienting and phosphorylation sites within tryptophan hydroxylase using homology-based molecular modeling. *J Mol Biol* **302**, 1005–1017.
 - 38 Yohrling GJ, Mockus SM and Vrana KE (1999) Identification of amino-terminal sequences contributing to tryptophan hydroxylase tetramer formation. *J Mol Neurosci* **12**, 23–34.
 - 39 Patel D, Kopec D, Fitzpatrick F, McCorvie TJ and Yue WW (2016) Structural basis for ligand-dependent dimerization of phenylalanine hydroxylase regulatory domain. *Sci Rep* **6**, 23748.
 - 40 Jaffe EK, Stith L, Lawrence SH, Andrade M and Dunbrack Jr RL (2013) A new model for allosteric regulation of phenylalanine hydroxylase: implications for disease and therapeutics. *Arch Biochem Biophys* **530**, 73–82.
 - 41 Zhang S, Hinck AP and Fitzpatrick PF (2015) The amino acid specificity for activation of phenylalanine hydroxylase matches the specificity for stabilization of regulatory domain dimers. *Biochemistry* **54**, 5167–5174.
 - 42 Lang EJM, Cross PJ, Mittelstädt G, Jameson GB and Parker EJ (2014) Allosteric ACTion: the varied ACT domains regulating enzymes of amino-acid metabolism. *Curr Opin Struct Biol* **29**, 102–111.
 - 43 Tenner K, Walther D and Bader M (2007) Influence of human tryptophan hydroxylase 2 N- and C-terminus on enzymatic activity and oligomerization. *J Neurochem* **102**, 1887–1894.
 - 44 Thórólfsson M, Ibarra-Molero B, Fojan P, Petersen SB, Sanchez-Ruiz JM and Martínez A (2002) L-phenylalanine binding and domain organization in human phenylalanine hydroxylase: a differential scanning calorimetry study. *Biochemistry* **41**, 7573–7585.
 - 45 Calvo AC, Scherer T, Pey AL, Ying M, Winge I, McKinney J, Haavik J, Thöny B and Martinez A (2010) Effect of pharmacological chaperones on brain tyrosine hydroxylase and tryptophan hydroxylase 2. *J Neurochem* **114**, 853–863.
 - 46 Royo M, Daubner SC and Fitzpatrick PF (2005) Effects of mutations in tyrosine hydroxylase associated with progressive dystonia on the activity and stability of the protein. *Proteins* **58**, 14–21.
 - 47 Walker PA, Leong LEC, Ng PWP, Tan SH, Waller S, Murphy D and Porter AG (1994) Efficient and rapid affinity purification of proteins using recombinant fusion proteases. *Nat Biotechnol* **12**, 601–605.
 - 48 Gasteiger E, Hoogland C, Gattiker A, Duvaud S, Wilkins MR, Appel RD and Bairoch A (2005) *Protein Identification and Analysis Tools on the ExPASy Server. The Proteomics Protocols Handbook*. Humana Press Inc., Totowa, NJ.
 - 49 Niesen FH, Berglund H and Vedadi M (2007) The use of differential scanning fluorimetry to detect ligand interactions that promote protein stability. *Nat Protoc* **2**, 2212–2221.
 - 50 Manning LR, Jenkins WT, Hess JR, Vandegriff K, Winslow RM and Manning JM (1999) Subunit dissociations in natural and recombinant hemoglobins. *Protein Sci* **5**, 775–781.
 - 51 Moran GR and Fitzpatrick PF (1999) A continuous fluorescence assay for tryptophan hydroxylase. *Anal Biochem* **266**, 148–152.

Supporting information

Additional Supporting Information may be found online in the supporting information tab for this article:

Appendix S1. Sequences of *hTPH2* protein variants.

Table S1. Primers for cloning the recombinant truncated *hTPH2* protein variants.

Fig. S1. Alignment of the regulatory domains of *hTPH2* and *rnPAH*.

Fig. S2. Representative example of raw data from differential scanning fluorimetry.

Fig. S3. SDS-PAGE results of collected peaks from purification of *rchTPH2* using Phe buffer.

Fig. S4. SDS-PAGE results of collected peaks from purification of *NΔ47-rchTPH2* using Phe buffer.

Fig. S5. SDS-PAGE results of collected peaks from purification of *chTPH2* using Phe buffer.